Continental Shelf Research 29 (2009) 759–774

Contents lists available at ScienceDirect

Continental Shelf Research

journal homepage: www.elsevier.com/locate/csr

Surface temperature, chlorophyll and advection patterns during a summer upwelling event off central Portugal

Paulo B. Oliveira [a,*], Rita Nolasco [b], Jesus Dubert [b], Teresa Moita [a], Álvaro Peliz [c]

[a] INRB/L-IPIMAR, Av. Brasilia, 1449-006 Lisboa, Portugal
[b] Centro de Estudos do Ambiente e do Mar (CESAM), Departmento Física, Universidade de Aveiro, 3810-193 Aveiro, Portugal
[c] Instituto de Oceanografia, Faculdade de Ciências, Universidade de Lisboa, Campo Grande, 1749-016 Lisboa, Portugal

ARTICLE INFO

Article history:
Received 2 May 2008
Received in revised form
31 July 2008
Accepted 6 August 2008
Available online 5 September 2008

Keywords:
Coastal upwelling
Primary production
Phytoplankton dynamics
Jet separation
Coastal retention
Hydrodynamic model
Lagrangian model
Northeast Atlantic
Portugal

ABSTRACT

Satellite-derived sea surface temperature (SST) and chlorophyll ([Chl]) concentration maps are used together with numerical models to study the advection patterns observed during a summer upwelling event off central Portugal, a region characterized by a complex coastline and bathymetry. It is shown that the model solutions realistically reproduce the main patterns of spatial and temporal SST variability, namely the 2–2.5 °C decrease in the active upwelling areas during the wind intensification phase, the 1-day lag between the peak of the northerlies and minimum SST, and the small SST variability in the sheltered embayments. The expected circulation features are reproduced in the model solutions: the strong along-slope flows, the development of filaments and separated jets, shadow areas downstream of main capes, frontal-scale instabilities and the rapid onset of coastal counter currents along the inshore zone during relaxation. The evolution of the oceanographic conditions, specifically the mixed layer depth and horizontal velocity, and the advection patterns obtained from a Lagrangian model are compared with the observed SST and [Chl] variability. The results imply that the potential phytoplankton accumulation/growth (PPAG) areas are characterized by surface temperatures lower than 16.5 °C, mixed layer depth and horizontal velocity less than 30 m and 0.3 m/s, respectively. It is shown that remotely-sensed [Chl] concentration patterns, namely its asymmetric distribution relative to SST during the intense wind phase, is primarily related to the mixed layer depth and secondly to the horizontal velocity. The trajectories obtained with the Lagrangian model confirmed earlier suggestions of the presence of recirculation cells, downstream of the capes where the coastal jet separates from the coast, and revealed that significant vertical displacements occur in these cells.

1. Introduction

The summer oceanographic conditions along the west Portuguese coast are dominated by the coastal upwelling driven by persistent equatorward winds. Previous works based on satellite-data (Fiúza, 1983; Haynes et al., 1993; Sousa and Bricaud, 1992; Peliz and Fiúza, 1999) have shown that the summer sea surface temperature (SST) and chlorophyll ([Chl]) patterns are similar to those observed in other coastal upwelling regions, characterized by the recurrence of cold pigment-rich filament structures extending offshore.

Among the various locations where filament structures recurrently appear, the area off central Portugal as attracted the attention of recent works, suggesting that the local conditions could favor the development of harmful algal blooms (Moita et al., 2003; Amorim et al., 2004). This area, extending roughly from 38°N to 40°N, is characterized by major changes in coastline orientation, irregular bottom topography and the presence of large estuary (Tagus), leading to complex flow patterns with active upwelling centres and shadow areas (Moita et al., 2003).

Recent results have highlighted the importance of the temporal and spatial structure of upwelling to understand the high levels of productivity of coastal upwelling systems. Temporal fluctuations, provided by alternating pulses of upwelling and relaxation, and spatial structuring provided by alternating upwelling at headlands and retention in bays, allow strong upwelling that favors nutrient delivery to be juxtaposed with less energetic conditions that favor stratification and plankton blooms (Largier et al., 2006). On the other hand, it has been proposed that geographical variability in eddy activity and mixing of offshore and nearshore waters is a key factor for explaining the observed variability in primary production of different upwelling regions (Marchesiello and Estrade, 2007). These results and the growing evidence of a large primary production variability at scales ranging from 2 to 100 km has

* Corresponding author. Tel.: +351 213 027 068; fax: +351 213 015 948.
E-mail address: pbo@ipimar.pt (P.B. Oliveira).

0278-4343/$ - see front matter © 2008 Elsevier Ltd. All rights reserved.
doi:10.1016/j.csr.2008.08.004

prompted the need to better understand the mechanisms by which the physical dynamics are reflected by the biological processes at such scales (Levy, 2008).

In this work we use satellite images and numerical model results to build up a framework under which relevant oceanographic features during an upwelling event off central Portugal (July 2005) are interpreted and discussed. Contrasting satellite data against the model solutions we show the model's ability to realistically reproduce the observed SST variability and describe the time evolution of the SST and [Chl] patterns. The results of a Lagrangian model are used to determine the impact of the shelf circulation on actual water displacements, to provide insight on potential origins and destinations of upwelled water and related them to the evolving SST and [Chl] patterns.

2. Data, models and methods

2.1. Satellite data

The satellite image sequences were constructed from various instruments with different space and time sampling capabilities. The SST maps were derived from SEVIRI (spinning enhanced visible and infra red imager, on board Meteosat), AVHRR (advanced very high resolution radiometer, NOAA satellite) and MODIS (moderate resolution imaging spectrometer, Aqua satellite) data, with nominal spatial resolutions respectively of 5, 2 and 1 km. SEVIRI and AVHRR SST products (CMS, 2005) were obtained from EUMETSAT's Ocean and Sea Ice Satellite Application Facility. The SST and [Chl] concentration maps derived from MODIS data (Feldman and McClain, 2006) were obtained from the Goddard's Space Flight Centre ocean colour data archive.

For the comparison between the satellite-derived and the model SST, the 3-hourly model temperatures of the top level of the model were linearly interpolated to the same spatial and temporal grid of the satellite images (~2 km). Moreover, only the valid (cloud-free) grid points (pixels) of the satellite images were considered for the model averages. Each model distribution interpolated for the time of the satellite pass was masked to retain only the same grid points of satellite image. SST time series were constructed for one offshore (area 0, Fig. 1) and three coastal areas with different responses to the wind forcing: the meridionally aligned coastal segment north of Cape Roca (area 1), the embayment between Capes Roca and Espichel herein referred to as Lisbon Bay (area 2) and the area between Capes Espichel and Sines herein Setúbal Bay (area 3).

2.2. Ocean model

The ocean simulations were performed using the Regional Ocean Modeling System (ROMS) described in Shchepetkin and McWilliams (2003, 2005), Wilkin et al. (2005), with embedded nesting capabilities, ROMS-AGRIF (Adaptive Grid Refinement In Fortran; Penven et al., 2006). ROMS is a 3D free-surface, sigma-coordinate, split-explicit primitive equation model with Boussinesq and hydrostatic approximations. ROMS-AGRIF enables the use of online and offline nesting thus permitting the regional applications to be built based on basin and local-scale configurations, and to cover a wide range of time and space scales. The present modeling experiments are a follow up of the Peliz et al. (2007a) numerical study, which the reader is referred to for a more thorough description of the model and of the approach used in the configurations. Herein we present a general overview.

The ocean model experiments are conducted using three domains; large, medium and small (LD, MD, SD) shown in Fig. 1. The initial and boundary conditions for the first domain (LD) are obtained from Peliz et al. (2007a) experiments from a first level of offline nesting. This domain of about 9 km resolution is intended to act like a buffer to downscale the basin scale variability (see Peliz et al., 2007a) into the Coastal Transition Zone. However, at this resolution the mesoscale is still poorly resolved. An additional grid of 3 km resolution (MD) is used to resolve the mesoscale, and in particular the Mediterranean outflow, its associated features like meddies, and its interaction with surface circulation. Finally, to solve frontal scale processes and coastal processes like river runoff and innershelf circulation features a third smaller domain (SD) with resolution in the order of 1 km is used (see in Fig. 1). The model bathymetry is based on National Geophysical Data Centre 2 min topography (ETOPO2) (Smith and Sandwell, 1997). The bathymetry depth data (h) is interpolated into model grids and smoothed several times until the factor $r = \delta h/2h$ (Haidvogel and Beckmann, 1999) is below 0.2. Sixty sigma levels are used with sigma resolution increasing near the surface ($\theta_s = 4$ and $\theta_b = 0$). Tidal elevation along the boundaries is included in LD (e.g. Marta-Almeida and Dubert, 2006), and point sources of mass (100 m^3/s), temperature (15 °C), and salinity (15) to simulate the Tagus river are imposed in SD grid. A realistic Mediterranean Undercurrent was imposed by a boundary inflow/outflow condition at the Strait of Gibraltar (see Peliz et al., 2007a for details). All grids communicate in 1-way nesting as described in Penven et al. (2006).

The experiments were conducted in two phases: a spin-up phase (May and June, 2005) with only LD and MD active and forced with low resolution atmospheric fluxes obtained from NCEP reanalysis (heat fluxes and solar shortwave radiation), and from QuickScat data (momentum fluxes). The second phase corresponds to the target simulation with all three domains, to approximate the June–August 2005. In this phase, high resolution atmospheric fields from WRF simulations (described below) are used. The results analysed in this paper correspond to this period and to the small domain (SD).

2.3. Atmospheric model

The Weather Research and Forecast atmospheric model (WRF V2.0) was used to dynamically downscale atmospheric reanalysis for the study period. WRF is a widely used research and forecast system (Skamarock, 2005) and an application of WRF simulations with ROMS is reported in Teles-Machado et al. (2007, e.g.). A regional configuration of WRF is set-up for the study period from June to August, 2005. The WRF simulations are initialised and forced along the open boundaries with the National Centre for Environment and Prediction (NCEP) reanalysis data (Kalnay et al., 1996). A grid of 15 km and 60 vertical levels is used. Surface winds, humidity, pressure, temperature and radiative data are calculated and passed to the ocean model for the air-sea fluxes calculation through a bulk formulation.

2.4. Lagrangian analysis

A Lagrangian submodel (floats for brevity) coupled to ROMS (Capet et al., 2004; Peliz et al., 2007b) is used for analysis of water parcel displacement. The floats use the 3D model velocity field for advection with a fifth-order scheme based on Adams-Bashforth/Adams-Moulton predictor–corrector time step algorithm. AGRIF has been adapted to manage the communication of floats through the different model domains (Capet et al., 2004).

A set of floats was initialized to obtain a Lagrangian description of the flow during the onset and relaxation of the upwelling event at time scales of interest for phytoplankton development.

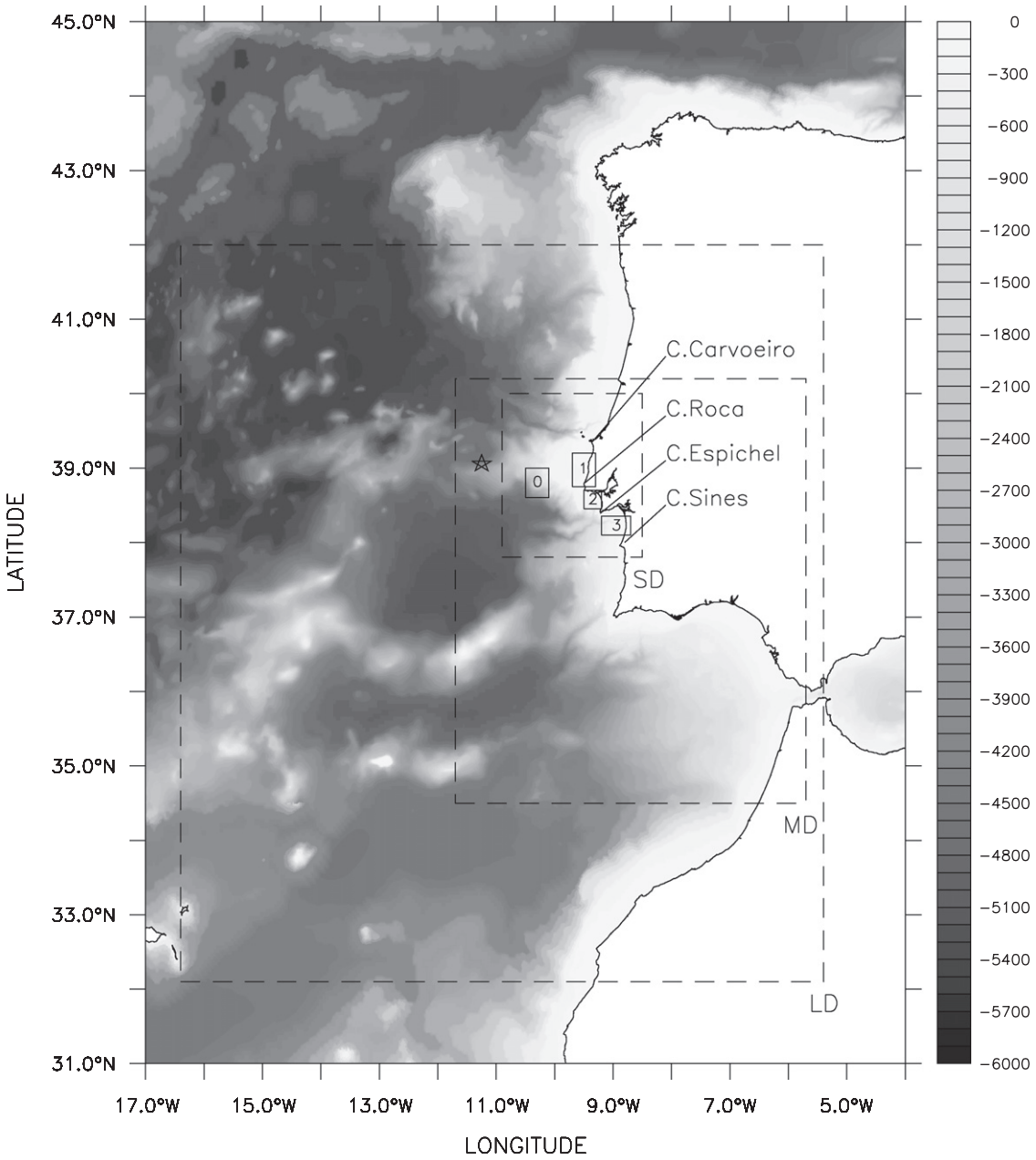

Fig. 1. Bathymetry of the study area, model domains and main capes. Dashed lines represent the geographical limits of the three nested model domains (LD, MD and SD). Labeled boxes (0–3) identify the areas selected to study the spatially averaged SST time series. Areas 2 and 3 are referred in the text as Lisbon and Setúbal bays. The star marks the NCEP grid point used to extract the large scale wind forcing represented in Fig. 2.

The floats were initialized as a fine grid of floats separated in the horizontal by 3 km. The southern, northern and western boundaries of the cluster of floats are 38.1°N, 39.8°N and 10.25°W, respectively. The floats extend from the boundaries to the coast, limited by the bathymetric level of the floats at the initial location. Five levels in the vertical are initialized, at depths from 10 to 50 m with step 10 m, in order to properly resolve the vertical displacements of the floats.

Two periods were analysed, the first during the maximum of the northerly winds, starting on July 4 and a second one, corresponding to the wind relaxation phase, in which a second cluster of particles were released on July 6. The float displacement was analysed three days after the release time, in order to create maps of displacement of the floats during that period, as detailed below.

3. Results

3.1. Wind evolution during the simulation period

One complete cycle of intensification and relaxation of upwelling favorable wind occurred in late June, early July 2005, embedded on the typical summer northerly wind regime (Fig. 2, top). The intensity of the northerly wind component remained greater than 5 m/s for a 8-day period, from June 30 to July 7, with peak velocities on July 4, exceeding 12 m/s in the offshore and meridionally aligned coastal segment north of cape Roca (area 1), being less intense in the two embayments south of this cape, particularly in Setúbal Bay (area 3) where the maximum northerly winds remained less than 8 m/s throughout the event (Fig. 2, bottom).

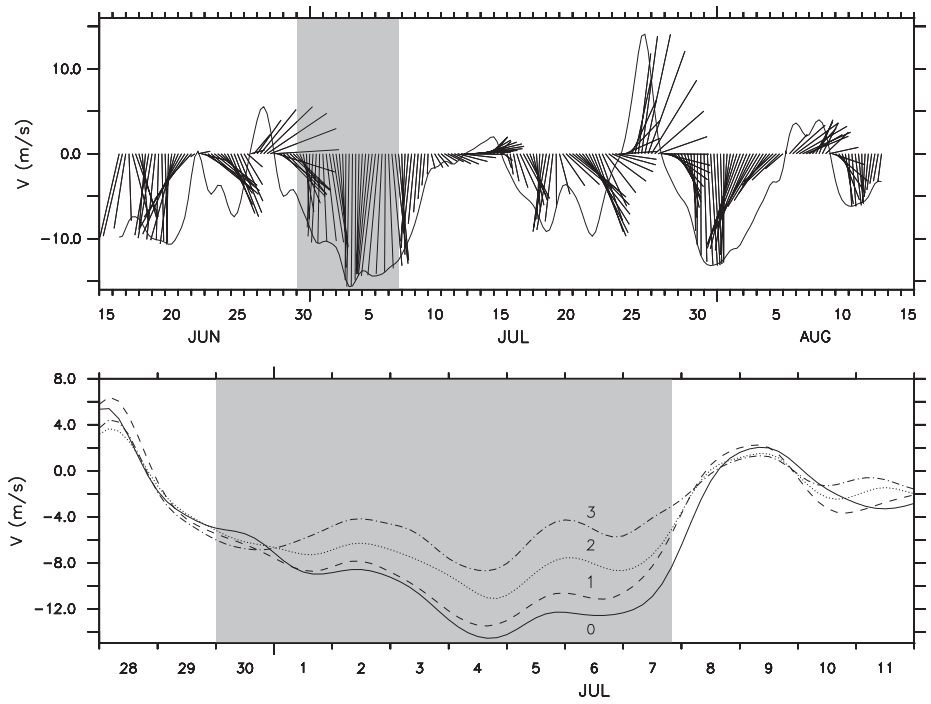

Fig. 2. Offshore wind regime in summer 2005 from NCEP reanalysis at 39.05N, 11.25W (stick diagram and N–S wind component, top) and spatially averaged N–S wind component for boxes 0–3 (bottom) (*cf.* Fig. 1). Grey area indicates the 8-day period (June 30–July 7) when the averaged N–S wind component in Lisbon Bay (area 2) was higher than 5 m/s.

3.2. Main spatio-temporal variability patterns

The time series of spatially averaged wind (meridional component of WRF—dashed line) and SST (meteosat—green; NOAA—red; model—blue) in four selected areas (cf. Fig. 1) are shown in Fig. 3. During the intensification of the northerly winds, from June 29 to July 4, there is a 2−2.5 °C SST decrease in the areas north of cape Espichel (areas 1 and 2), in contrast with the smaller variation observed in Setúbal Bay where warm temperatures persist throughout the intensification and relaxation cycle (Fig. 3). In this area, the amplitude of the SST fluctuations is similar to that of the offshore area, where the difference between the satellite and model SST is within the range of the diurnal SST variability (cf. dots in Fig. 3). The time scale and phase of the cooling and warming cycle are well reproduced by the model (blue line) that nevertheless shows a slightly lower SST (∼0.5 °C) in area 1. In this area, minimum surface temperatures are attained about 1-day after the peak of the northerlies, remaining low for about two days. On July 7 there is a strong decrease in the northerly wind component that coincides with an almost synchronous (less than one day) SST warming in all areas, including the offshore area and the coastal area north of Cape Roca where the wind speed was still as high as 6 m/s. This warming is faster and stronger in the satellite data than the model, leading to a larger difference between the satellite and model SST at the end of the upwelling event for low wind speeds.

To analyse the upper layer response to the wind event, the time-averaged and corresponding standard deviation (*SD*) maps (Fig. 4a) were calculated for the 8-day period of stronger northerly winds (June 30–July 7—gray bar in Fig. 2). Mean SST fields show the typical SST signature of coastal upwelling along the meridionally aligned coast north of Cape Roca, with a cold water band along the coast and two sharp filaments rooted at Capes Carvoeiro and Roca—herein referred to as the Carvoeiro and Roca filaments.

The signature of the filaments is also clearly marked in the *SD* fields (Fig. 4b), particularly their offshore boundaries, with high *SD* values. The embayments south of cape Roca are both characterised by warmer and less variable SST, particularly in Setúbal Bay where a conspicuous warm water pool is observed, with average SST values as high as offshore and variability confined to a narrow coastal band.

For the period of intense winds, Fig. 4e and f show that the higher mean [Chl] values are located in the shelf areas occupied by colder waters, being maximum in the southern filament boundaries, particularly south of the Carvoeiro filament where both average and *SD* values are high. On the other hand, the two adjacent embayments south of Cape Roca are marked by contrasting [Chl] patterns, with high average values in Lisbon Bay and values as low as in the open ocean in Setúbal Bay, which is also an area of low temporal variability. The coupling between the SST and [Chl] fields is described in greater detail in Section 3.4.

In general terms, the average and *SD* maps computed from the top-layer model results, interpolated to the same spatial and temporal resolution of the satellite data (Fig. 4c and d), show that the model reproduces the same structures, particularly the signature of the two cold filaments, the warmer and less variable SST in Lisboa and Setúbal bays, and the narrow coastal band of higher *SD*.

3.3. Filament dynamics and internal structure adjustment

The averaged SST patterns presented above correspond to the expected circulation features associated with coastal upwelling in a region of complex coastal morphology with the development of a strong alongshore coastal jet interacting with topography. Fig. 5 illustrates the main dynamical structure of the event (averaged over the same 8-day period: June 30–July 7) using the model velocities, temperature and density fields. The upper left panel

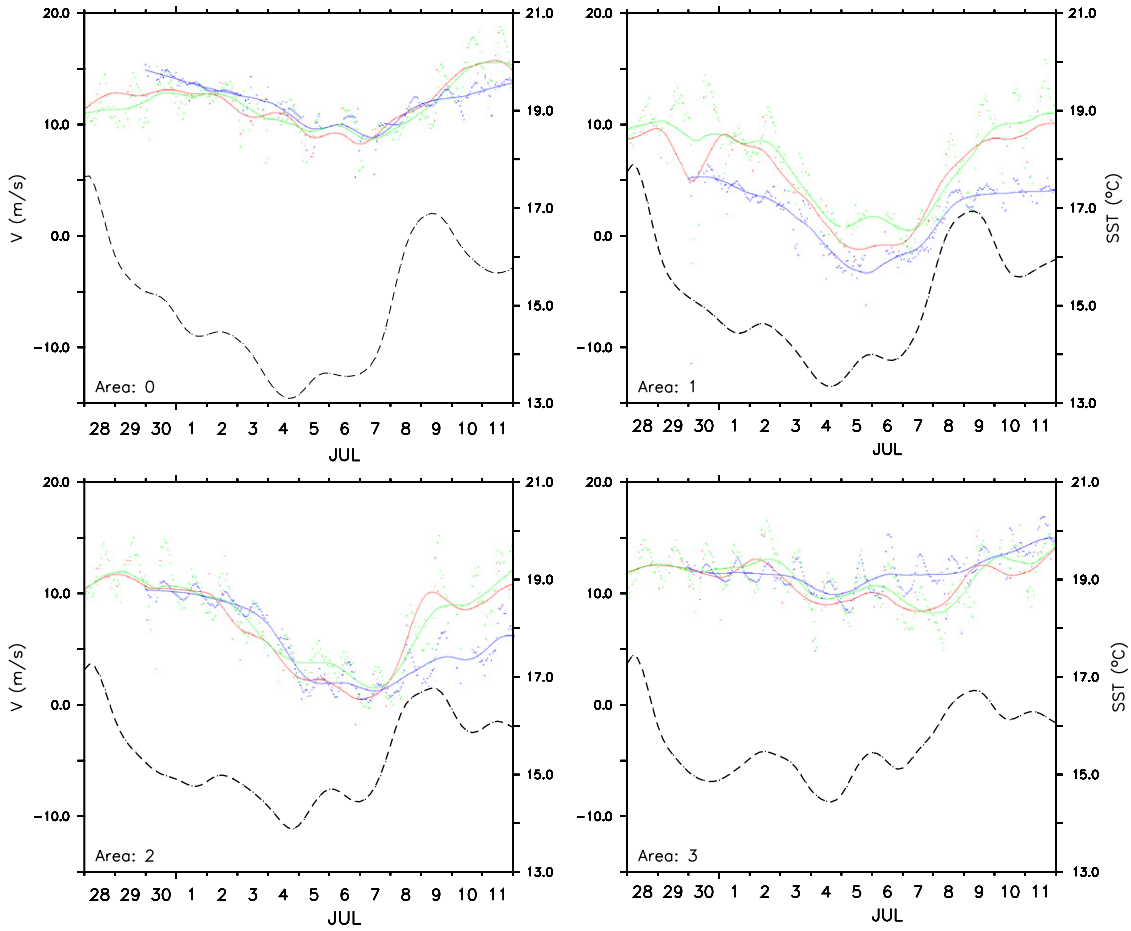

Fig. 3. Spatial average time series for areas 0–3 (*cf.* Figs. 1 and 4a) of WRF N/S wind component (dashed line, left axis) and SST from satellite and model (solid lines, right axis). Dots represent the average values for each individual image (model output of 3h) and solid lines a 2-day running mean. Colors/line-types represent the different sources: model–blue/small-dashes, METEOSAT–green/long-dashes, NOAA–red/dash-dot.

represents the topography of the $\sigma_T = \rho(S,T,0) - 1000 = 26.6$ isopycnal (representative of the top of the thermocline, colour shading), the free surface topography (thin contour) and the upper surface 10–30 m layer (representative of the mixed layer—ML, arrows) velocity vectors. The upper right panel represents the average mixed layer depth and the euphotic depth (Z_e) computed from the 8-day average [Chl] concentration, using the formula proposed by Morel and Berthon (1989).

The zone of most marked uplift of the isopycnals and stronger jet corresponds to the coastal band north of Cape Carvoeiro. Downstream of the Cape the jet clearly separates and the coastal zone south of the Cape corresponds to the zone of generation of a second jet though the elevation of the isopycnal surface is smaller. This second jet separates downstream the Roca Cape, giving rise to the Roca Filament. The separation of both jets is accompanied by the formation of cyclonically rotating pools of dense water inshore. These circulation features are clearly reflected by the depression in surface elevation and the upward displacement of the $\sigma_T = 26.6$ isopycnal which rises from about 50 m offshore to less than 15 m south of Cape Roca, the same happening in the lee of cape Carvoeiro although the deformation of the isopycnal field has a smaller horizontal extent. This adjustment of the internal field is clear in the zonal sections of temperature crossing the filaments (Fig. 5c and d). In the vertical sections it is possible to observe the core of the filaments (in the velocity field) which correspond to a breakup of the stratification, and the uplifted isothermals in the inshore side of the filament. In the Roca case, the spatial scale of the deformation is in the order of 20–30 km (an expected value for the internal radius of deformation), consequence of the geostrophic adjustment of the density field to the separated jet protruding southward.

Inshore of the separated jets, the density surfaces have a conspicuous doming shape associated with cyclonic circulation (Fig. 5a) cells. These features are characterised by poleward velocities along the inshore face of the domes, reaching 5 cm/s just above the thermocline, and surface intensified equatorward jets along the offshore face of the domes, up to 25 cm/s at the surface (Fig. 5b and c). An additional consequence of the dynamics is the isolation of the bays from the main southward upwelling current. The Lisboa bay is affected by cyclonic recirculation and a small (possibly local) southward flow on the eastern edge of the bay. In the case of Setúbal bay there is a reemergence of the southward current (see Fig. 5a at 38.2°N) but no significant elevation of the isothermals is produced. Another important distinction between the two embayments is the anticyclonic circulation in Setúbal bay associated to a surface elevation high.

There is a general similarity between the topography of the $\sigma_T = 26.6$ isopycnal and the mixed layer depth (Fig. 5a and b), with exception of the coastal areas between capes Roca and Carvoeiro where the isopycnal is shallow and the mixed layer is thicker. Above the domes the mixed layer, defined as the depth where the temperature is 0.5 °C below the average 0–10 m average, is relatively shallow, particularly in Lisbon bay where it is only 10–15 m deep.

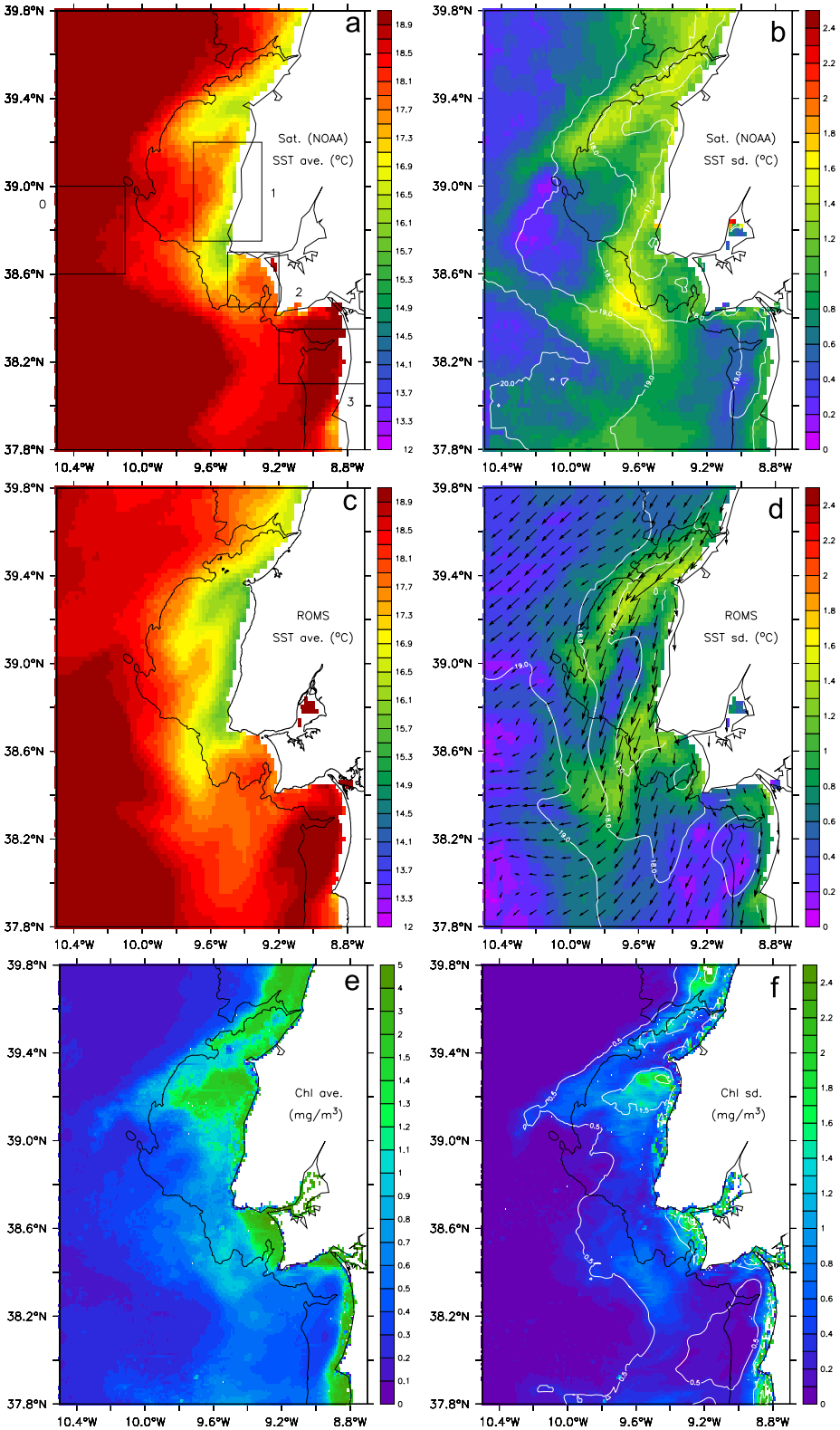

Fig. 4. Average (left) and standard deviation (right) of satellite SST (a,b), model SST (c,d) and chlorophyll (e,f) for the 8-day period (June 30–July 7 2005) of intense northerly winds. White contours overlayed on right panels were drawn from the average field shown on the left. The solid black line represents the 200 m bathymetric contour and the rectangular boxes on (a) show the position of the areas selected to compute the spatial averages relative to the SST features (same as in Fig. 1). Vectors overlayed on model SST standard deviation (d) are the 8-day average velocity of the top layer of the model.

The spatial patterns of SST *SD* (Fig. 4b and d) show that most of the observed temporal SST variability, from June 30 to July 7, is along the coastal areas where the temperatures drop due the upwelling of cold subsurface waters, and along the separated jets that transport the colder water offshore. The relatively high mean SST (Fig. 4a and c) but also high *SD* values along the coast south of

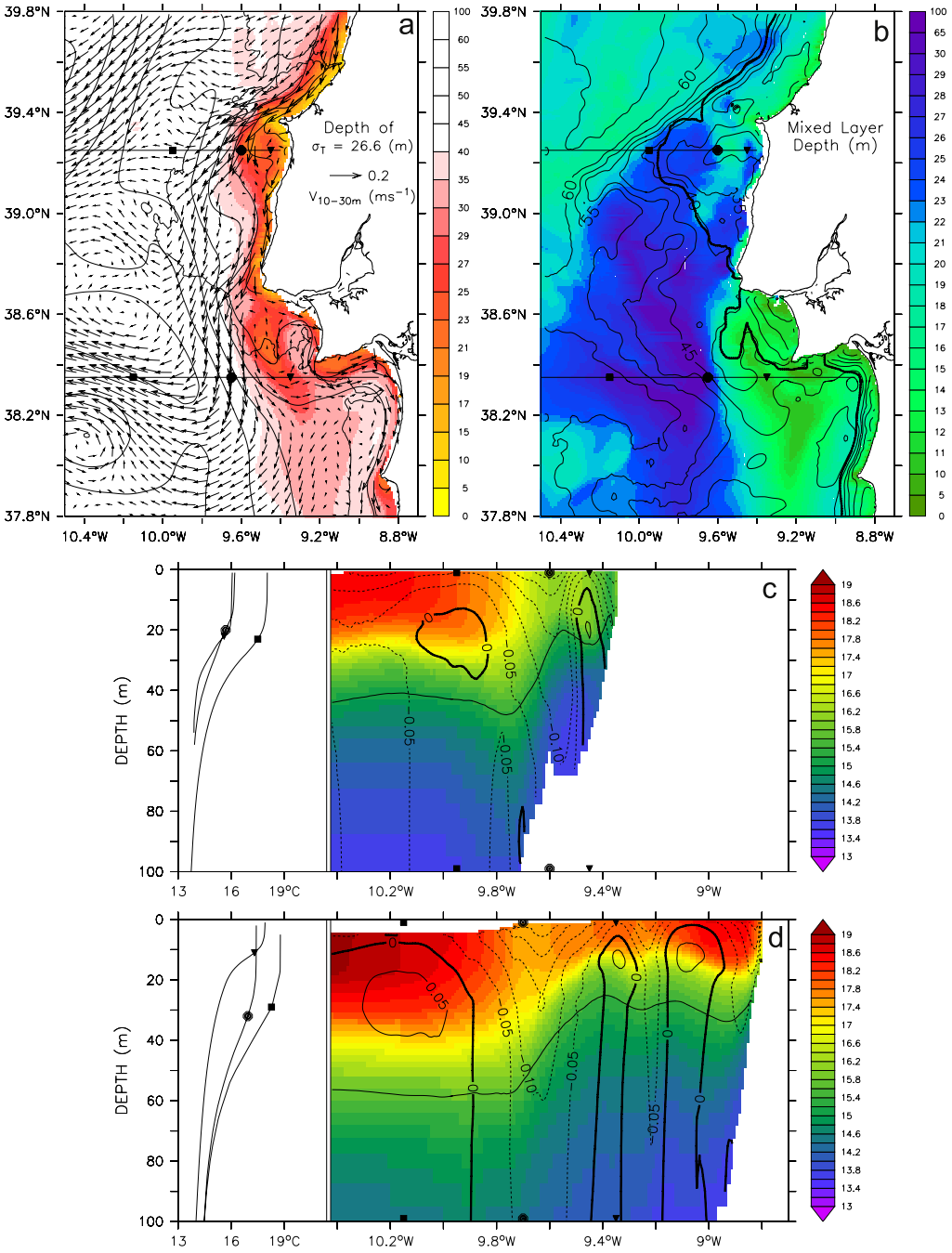

Fig. 5. Model solution for the topography of the $\sigma_T = 26.6$ isopycnal (a); mixed layer depth (b); and vertical temperature sections along zonal transects at 39.35°N (c), 38.25°N (d), drawn from 8-day (June 30–July 7 2005) averaged fields. Vectors in (a) represent the 8-day average velocity of the 10–30 m layer. The solid black lines and symbols overlayed in (a) and (b) map mark the position of the zonal transects and locations of vertical temperature profiles. Contours represent the average surface elevation (1 cm interval) and the 200 m isobath (thick) in (a); the euphotic depth Z_e (m) and area with average [Chl] greater than 1 mg/m^3 (thick) in (b); N/S velocity component in m/s (solid-poleward, dashed-equatorward) and the $\sigma_T = 26.6$ isopycnal in (c, d). Vertical temperature profiles at the selected locations are represented to the left of the zonal sections (c,d). The symbol position on the vertical profiles indicates the mixed layer depth, defined as the depth where the temperature is 0.5 °C less than the average 0–10 m layer temperature.

cape Roca suggest that upwelling is either less intense/persistent in these areas, however mean [Chl] values are similar or even higher to the coastal areas north of the cape with much lower mean SSTs.

Using the areas of high SST *SD* as a proxy of filament location and extension, Figs. 4b and d show that the model is able to realistically reproduce the filaments, with most differences being located offshore where filaments interact with the off-shelf mesoscale eddy field. This is the case of the offshore area south of Cape Espichel where an anticyclonic eddy centred at 38.2°N, 9.8°W should be responsible for the frontal structure at the shelf edge west of that Cape and the filament advection in the southeast direction.

3.4. *Time evolution of SST, [Chl] and circulation patterns*

The time evolution of daily averaged model SST, velocity vectors of the top 20 m, zonal temperature sections and MODIS [Chl] concentration throughout the upwelling event is presented

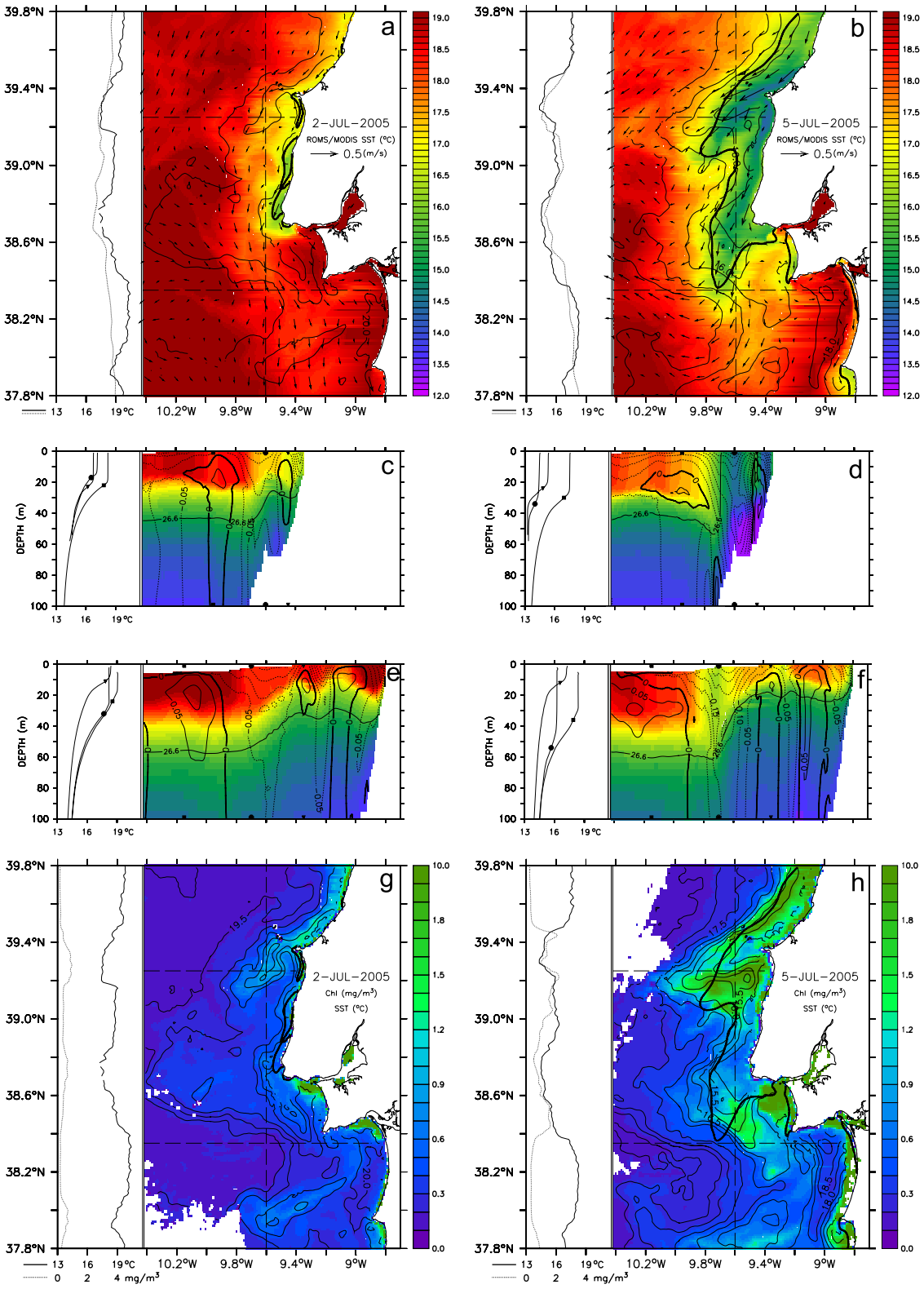

Fig. 6. Daily averaged model (shade) / satellite (contour) SST and surface velocity vectors of the top 20 m (top); zonal temperature, 26.6 isopycnal and N/S velocity sections (middle) and MODIS [Chl] concentration (bottom) with superimposed MODIS SST contours and model 16.5 °C isotherm of 0–10 m layer (thick) for July 2 and 5 2005. On the left of each surface map are represented meridional profiles along 9.6W: MODIS SST (solid) and model SST (dotted) next to the SST/surface velocity map, and the same MODIS SST data together with the [Chl] profile (dotted) next to the [Chl] map. Zonal temperature sections and profiles were drawn following the same criteria as in Fig. 5.

in Figs. 6 and 7. To provide a quantitative representation of SST and [Chl] values, meridional profiles along 9.6°W (cf. vertical dashed line on the maps) of variable pairs are presented on the left of the SST maps and [Chl] maps: satellite and model SST next to model SST map (a,b) and satellite SST and [Chl] on the [Chl] map (g,h). Contours overlaid on model SST maps were drawn from the daily SST average computed from the NOAA AVHRR data and contours on [Chl] maps are the synoptic MODIS

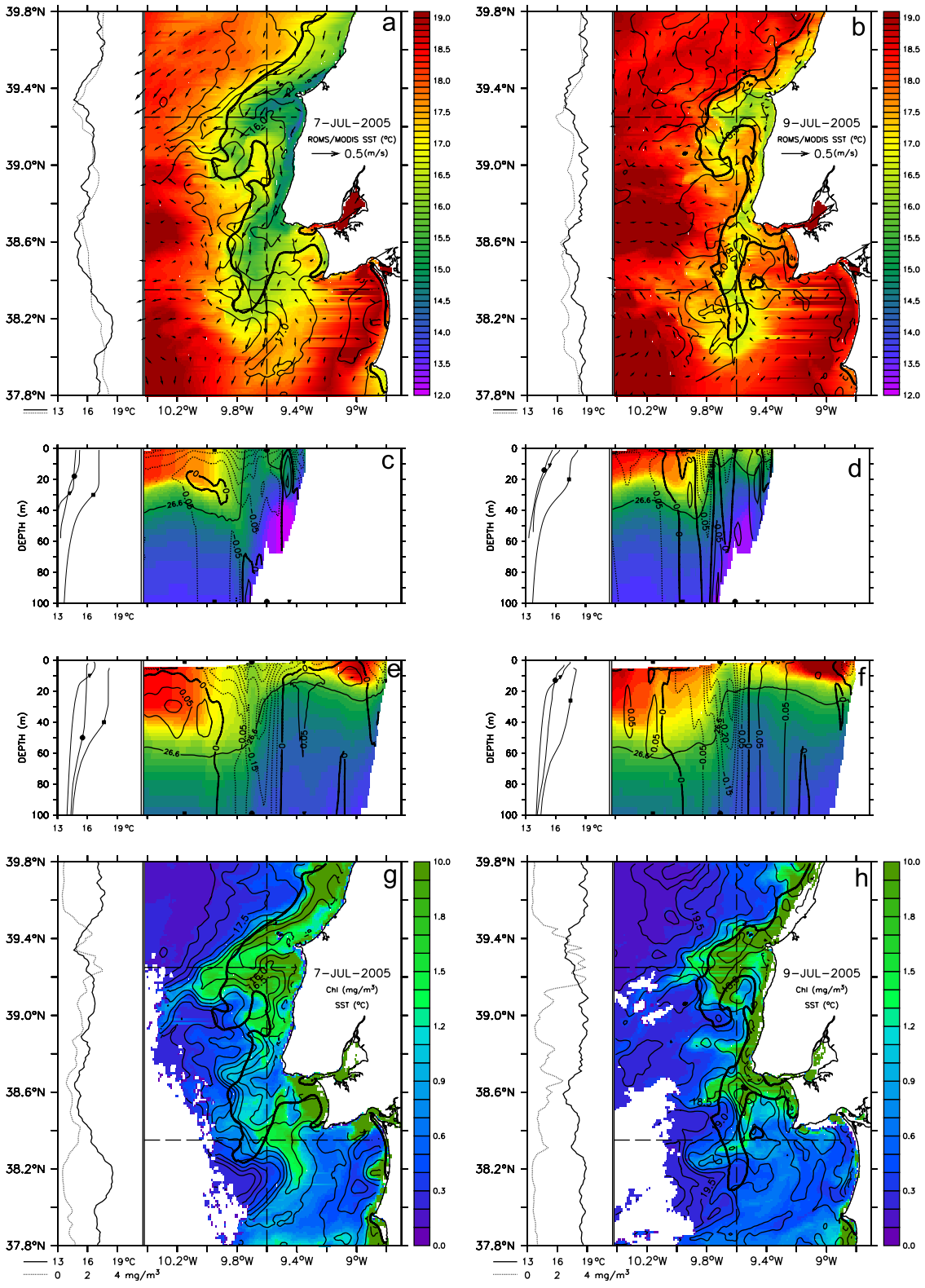

Fig. 7. Same as Fig. 6 but for July, 7 and 9, 2005.

SST from the same satellite pass. Contours and symbols overlaid on the zonal temperature sections (c–f) and vertical profiles follow the same criteria as in Fig. 5. The time evolution of the MLD, daily depth-averaged MLD horizontal speed ($V_{MLD} = \sqrt{u^2 + v^2}$) and topography of the $\sigma_T = 26.6$ isopycnal and surface elevation (as in Fig. 5) is shown in Fig. 8.

3.4.1. *Intensification phase*

At the beginning of the upwelling event, on July 2, after two days of northerlies higher than 5 m/s, a narrow band of colder waters (<18 °C) is observed north of cape Roca, with two small protrusions rooted at capes Carvoeiro and Roca. The [Chl] concentration is generally low (less than 1 mg/m^3, cf. meridional

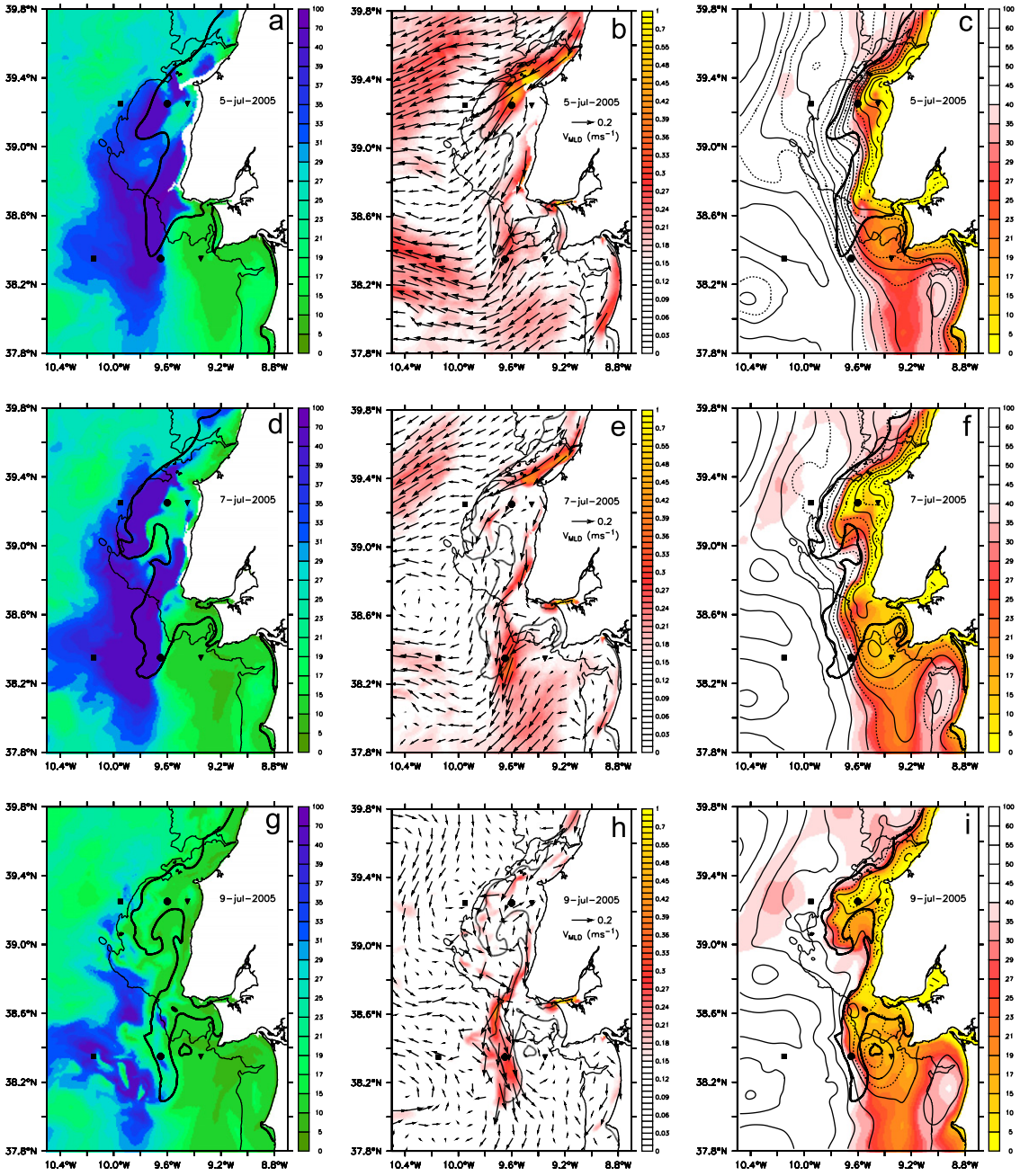

Fig. 8. Time evolution of daily mean mixed layer depth (MLD, left), MLD horizontal current speed ($V_{MLD} = \sqrt{u^2 + v^2}$) (middle) and topography of the density anomaly surface $\sigma_T = 26.6$ (right, as in Fig. 5). Contours represent the 200 m isobath, average surface elevation (c, f, i; solid contour spacing of 1 cm) and the 16.5 °C isotherm (thick) of the daily, 0–10 m, average model temperature as in Figs. 6 and 7. Vector arrows overlayed on the MLD horizontal speed represent the daily, depth averaged, mixed layer velocity. The results for July 5, 7 and 9 at 12:00 are presented in each row.

profile in Fig. 6g), being slightly higher in the areas of low SST. The main features of the vertical temperature distribution and N/S velocity component identified in Fig. 5 are already clearly identifiable at this date. The main differences are the lower intensity of the equatorward separated jets and the poleward sub-surface inshore current in the northern section.

The results for July 5 (Fig. 6, right) show that the intensification of the northerlies led to a SST decrease of about 4 °C along the axis of the two cold filaments, and an increase of MLD of about 20 m in offshore positions of the northern section, with outcrop of the 26.6 isopycnal, while in the southern section the MLD increases about 30 m in the westernmost position. A two-fold increase (from 0.15 to 0.30 m/s) of the equatorward flow intensity is observed in both sections along the axis of the separated jets.

There is a general [Chl] increase with a conspicuous spatial relationship with SST. Although being generally higher coastward of the 16.5 °C isotherm, [Chl] values are lower along the axis of the filaments, where the horizontal current speed exceeds 0.3 m/s (Fig. 8b), and higher in their periphery, particularly along the southern boundaries where values reach 2.5 mg/m^3 (Fig. 6h). These patterns have a close relationship to those of the MLD as show in Fig. 8a, with higher [Chl] values where the mixed layer is shallow and low [Chl] values for thicker mixed layers. This is particularly evident along the coastal segment between capes Roca and Carvoeiro, an area where the MLD exceeds 30 m.

Maximum horizontal velocities in the mixed layer coincide with minimum SST values along the coast and filament axis which is also the location of a drop in surface elevation and where the

$\sigma_t = 26.6$ isopycnal is shallower than 10 m (Figs. 8b and c). In addition to the rise in the coastward direction, Fig. 8c also shows that this isopycnal is above 20 m in Lisbon bay, inshore of the Roca filament (as marked by the 16.5 °C isothermal), corresponding to the formation of the density dome described in Fig. 5. This density field adjustment, represented by the upward tilt of the 26.6 isopycnal shown in the southern zonal section (Fig. 6f) is associated with the jet intensification and a weak poleward flow below the shallow mixed layer.

3.4.2. Relaxation phase

Three days after peak wind intensities (July 7), just before the northerly wind component becomes less than 5 m/s, the spatial SST and [Chl] structures (Fig. 7a, b and g, h) are similar to those observed two days before, with slightly higher [Chl] values and smoother meridional gradients, namely at the northern boundary of the Carvoeiro filament (~39.5°N) and south of the Roca filament (~38.4°N). As on July 5, the higher [Chl] values are generally bounded by the 16.5 °C isotherm. The [Chl] increase is more evident in the southern/inshore boundaries of the filaments, particularly south of Cape Carvoeiro, where both the satellite and model SST show the persistence of a warm water wedge between the filament and the coastal cold water band which is, in turn, an area where the MLD is less than 30 m (Fig. 8d). Co-located [Chl] and SST minima are still observed along the filament axis (cf. meridional profiles in Fig. 7g) where either maximum horizontal speeds are observed, as in the case of the Carvoeiro filament were mean ML horizontal speed exceeds 0.30 m/s (Fig. 8e), or the MLD is greater than 30 m as in the offshore part of the Roca filament (Fig. 8d).

A general upward displacement of the $\sigma_t = 26.6$ isopycnal is observed on July 7 (Fig. 8f), with most rise occurring along the coast, the filament axis and along their southern/inshore boundaries. The density dome located inshore of Roca filament becomes more prominent and extends in the equatorward direction, from cape Roca till the southern boundary of the model domain, acting as an offshore boundary of the anticyclonic cell that dominates the mixed layer circulation in Setúbal Bay where SST is high and [Chl] is low throughout the event. The spatial distribution of the surface elevation is similar to the isopycnal topography with troughs/crests above the density elevations/depressions, with the exception of a small area centred at 38.6°N, 9.6°W where both the isopycnal and surface elevation have a local trough.

At the end of the event on July 9, under calm wind conditions, there is a general SST increase with high spatial heterogeneity (Fig. 7b), associated to the restratification of the upper layers, including the filament areas, and the poleward advection of the warmer waters at the southern/inshore filament boundaries (Fig. 7b,d and f). The SST signature of these poleward flows is particularly clear in the vicinities of cape Espichel, where the warm water from Setúbal bay turns around the cape and occupies the southern part of Lisbon bay, having a striking resemblance with the observed [Chl] distribution, showing the same pattern of northward flow of oligotrophic waters (Fig. 7h). This symmetry between the warm/cold SST and low/high [Chl] patterns contrasts with the patterns of the previous days. [Chl] maxima are now observed along the coastal band and filament axis, particularly to the north of cape Roca and the Carvoeiro filament where there is two-fold [Chl] increase from values close to 2 mg/m^3 to about 4 mg/m^3 (cf. meridional profiles in Fig. 7h).

The restratification process is accompanied by the shallowing of the mixed layer (Fig. 8g), which mainly occurs along the coastal band north of cape Roca and the northern part of the Carvoeiro filament where a decrease of the horizontal ML speed is observed (Fig. 8h). At the end of the event the strongest ML horizontal speeds are located at the offshore and southern boundaries of the Roca filament, contouring the area of minimum depth of the 26.6 isopycnal and low surface elevation (Fig. 8h and i), where the circulation is cyclonic.

3.5. Potential phytoplankton accumulation/growth areas and pathways

The sequence of [Chl] maps and associated physical conditions described above showed a close relationship between [Chl], SST, MLD and horizontal MLD velocity. Taking into account that the observed satellite-derived phytopigment concentration variability may either result from phytoplankton accumulation or growth (PPAG), the results obtained here suggest that, during a summer upwelling event off central Portugal, the potential PPAG areas are characterised by the following physical (daily averaged) conditions: (i) surface (0–10 m) temperature lower than 16.5 °C; (ii) mixed layer shallower than 30 m (MLD <30 m: the average euphotic depth of the area where the 8-day average [Chl] is greater than 1 mg/m^3, thick contour in Fig. 5b); (iii) moderate horizontal advection, mixed layer horizontal current speed ($V_{MLD} = \sqrt{u^2 + v^2}$) not exceeding 0.3 m/s.

The PPAG areas computed from the application of the above physical constrains to the model solutions for July 7 and 9, when maximum phytoplankton concentrations occur, are presented in Fig. 9 (top), together with the areas where [Chl] >1.5 mg/m^3 (bottom) derived from Figs. 7g and h. The figure shows that the spatial patterns of the model-derived PPAG areas and the high satellite-derived [Chl] areas are very similar, namely the phytoplankton-rich areas south of capes Carvoeiro and Roca and the poor areas along the filament axis and the coastal segment north of cape Roca on July 7. The main differences are found in the offshore boundary of the Carvoeiro filament on July 7 where, apart from a spatial offset, satellite [Chl] is high but the model ML is thicker than 30 m and therefore is not considered a PPAG area. Another aspect that emerges from Figs. 9c and d is the 1.5 °C increase in the value of the satellite sea surface isotherm that bounds the high [Chl] areas, while the 16.5 °C of top 10 m of the model remains as a good proxy for cold-upwelled waters favorable to phytoplankton accumulation/growth, which is likely related both with a slow model restratification and a satellite SST bias due to diurnal warming under the low wind speed conditions observed on July 9.

To provide insight on the origin and pathways of the water parcels found in the pigment-rich areas south of cape Carvoeiro, Figs. 10 and 11 show the 3-day trajectory hindcast of the floats found in two destination areas and depths shallower than the average MLD, at 12:00 of July 7 (a,b) and July 9 (c,d), selected from the trajectories of all floats released on July 4 and 6, respectively. The destination areas selected were the PPAG areas presented in Figs. 9a and b (green contour in Figs. 10 and 11) and an area common to both dates (July 7 and 9) where the 4-day (July 6–9) average temperature in the top 10 m is less than 16.5 °C (black contour in Figs. 10 and 11). The average MLD (herein simply MLD), used to separate the trajectories of the floats according to their release depth, was computed over the same 4-day period. The trajectories of the floats whose release depth was shallower than the MLD are presented in Figs. 10a and c, and trajectories of the floats that upwell from depths deeper than 10 m below the MLD are presented in Figs. 10b, d and 11. The origin of the floats is marked with a circle/triangle if their destination is inside/outside the PPAG areas and their trajectories drawn in blue/light_blue in Fig. 10. Symbol colour represents the initial depth according to the colour-scale presented in each panel. In Fig. 11 the trajectories are coloured according to the evolution of float depth.

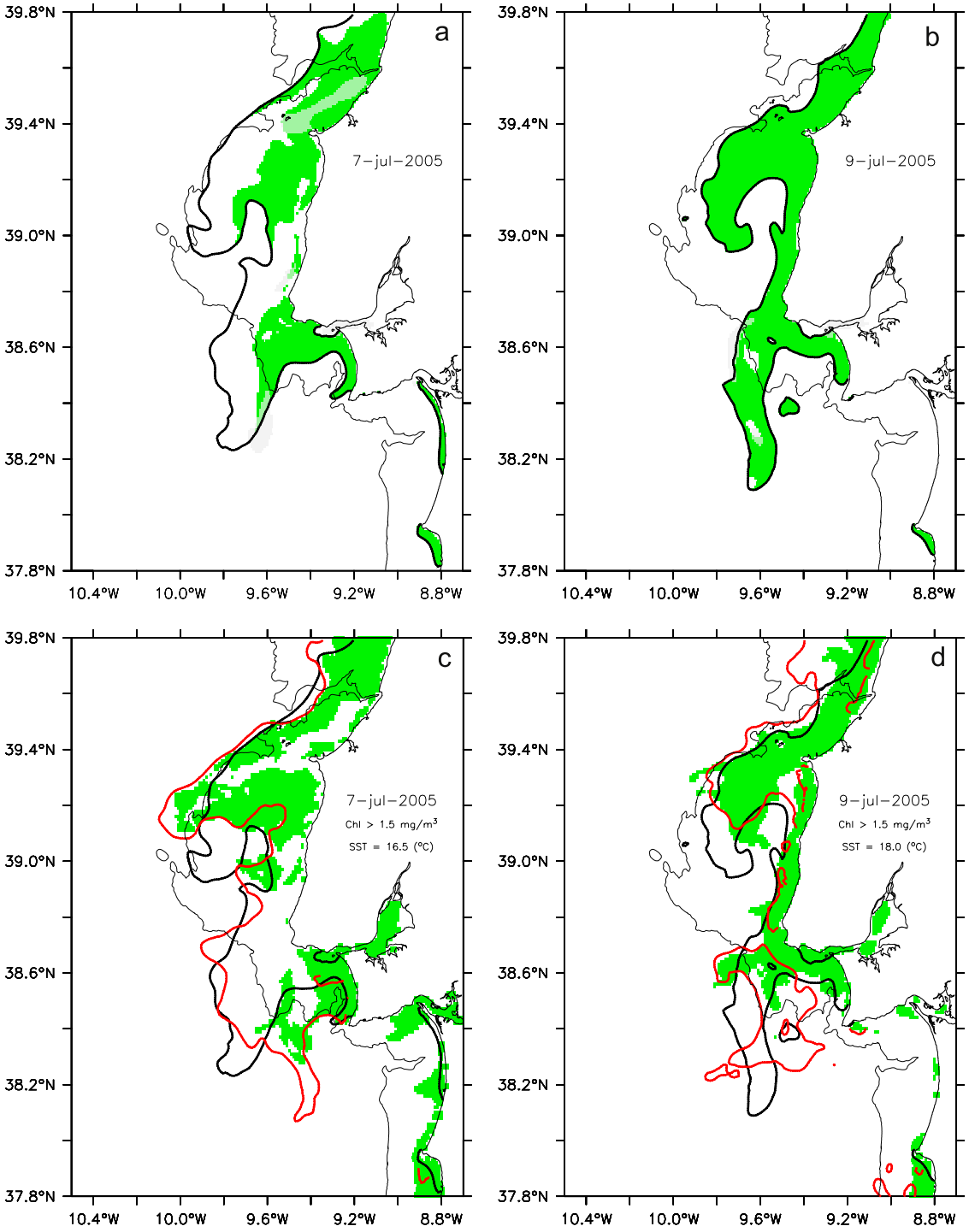

Fig. 9. Areas of potential phytoplankton accumulation/growth—PPAG—estimated from the model outputs (top), and areas where satellite-derived [Chl] are greater than 1.5 mg/m^3 (bottom). PPAG areas are defined as the areas occupied by cold-upwelled water ($T_{0-10\,m} < 16.5\,^{\circ}C$, thick contour—top), mixed layer shallower than 30 m (MLD <30 m, dark green/gray—top); and moderate horizontal advection (ML horizontal current speed <0.3 m/s, light green/gray—top). The results for July 7(a) and 9(b) at 12:00 were obtained using the previous 24-h averages of the three fields. Thin contour in all panels represents the 200 m isobath. Red/rugged contour in (c) and (d) represent the satellite SST isotherms 16.5 °C and 18.0 °C, respectively.

The results for 7 July clearly show that the PPAG areas just south of the capes are populated by floats that either recirculate in the ML (Fig. 10a) or locally upwell (almost all blue tracks representative of the floats arriving at PPAG areas are confined within, Figs. 10a, b). This is particularly evident south of cape Roca where most ML floats and those that upwell into the ML have their origin inside Lisbon Bay, from depths of 20–30 m, slowly rotating anticlockwise around a local trough of the $\sigma_T = 26.6$ isopycnal feeding the inshore side of the filament (Fig. 11b), in contrast with the offshore side which is mainly occupied by floats that upwell north of the cape and are quickly advected southward by the coastal jet (Fig. 10b), a feature also observed in the Carvoeiro area. The floats that upwell south of this cape on July 7 are organised in two groups: one just south the cape, inside 16.5 °C contour, and a second partially outside the area of low SST. The absence of the first group in the results of 9 July (Fig. 10d, 11c)

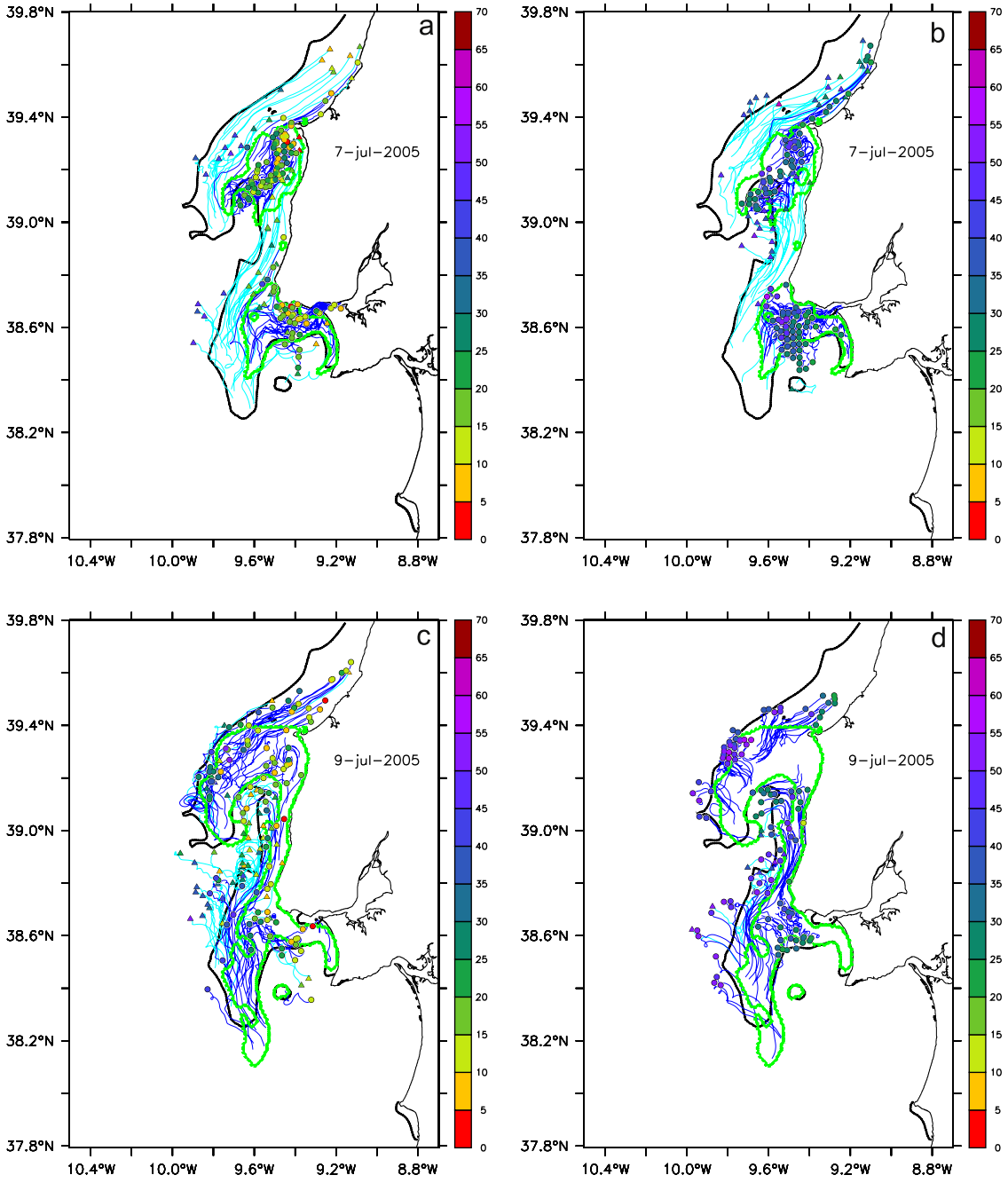

Fig. 10. Three-day trajectory hindcast of floats located in the area where the 4-day (July 6–9) average temperature in the top 10 m is less than 16.5 °C (thick contour) and depth is shallower than the 4-day mean MLD, on July 7 (top) and 9 July (bottom) at 12:00. The trajectories of the floats located inside/outside the PPAG areas south of capes Carvoeiro and Roca (green-rugged contour) are coloured in blue(solid)/light_blue(dotted) and their origin marked with a circle/triangle coloured according to the release depth. The trajectories of the floats released at depths shallower than the 4-day mean MLD are presented on the left and the floats that upwelled from depths 10 m below the MLD are resented on the right.

reveals that the circulation structures responsible for the vertical movement of waters parcels have different timescales. Upwelling close to the cape takes place over a shorter period than further offshore.

On July 9 there is a larger number of floats having their origin inside the low SST area (cf. 16.5 °C contour) owing to the smaller horizontal velocities. This is particularly clear along the coastal segment north of cape Roca where most floats released there are swept offshore during the period of intense winds, irrespective of their release depth, and therefore not shown in the results for July 7 (Figs. 10a, b). On July 9, the floats that upwell inside Lisbon bay (Fig. 11d) follow similar trajectories as on July 7, rotating anticlockwise around the isopycnal trough southwest of the cape that evolved to an isolated feature of the density field. Despite that the analysis of the dynamics is not in the scope of this work, it is interesting to note that this flow direction is contrary to the expected from the thermal wind balance, but is consistent with the local trough in surface elevation shown in Figs. 8f and i, suggesting that the flow in in this region is primarily adjusted to the barotropic pressure gradient.

As the upwelling relaxation progresses, the floats that upwell in the periphery of the Carvoeiro filament follow different pathways as shown in Fig. 11. On July 7, most floats released at depths 30–40 m upwell in a zone where the $\sigma_T = 26.6$ isopycnal is

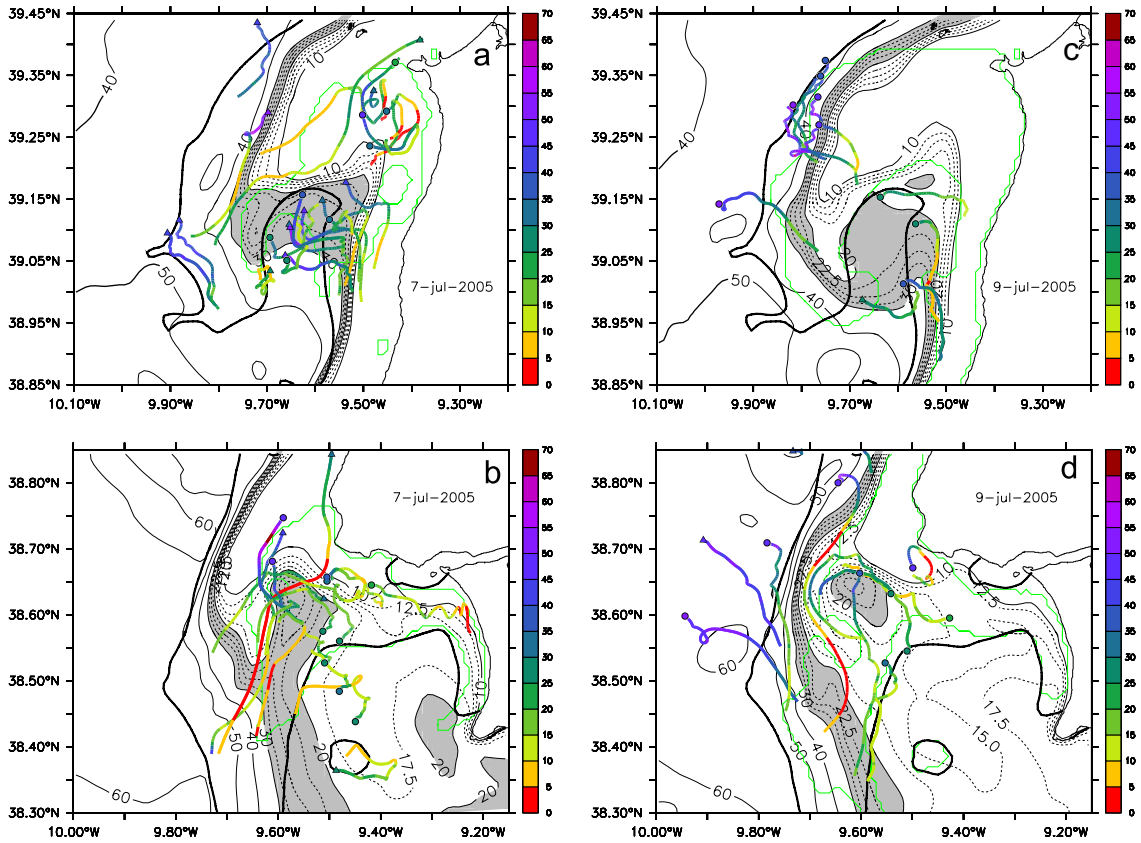

Fig. 11. Sample of 3-day trajectories drawn according to the same rules used in Fig. 10 b and d, for the areas south of capes Carvoeiro (top) and Roca (bottom), overlayed on (same) 3-day average depth of the density anomaly surface $\sigma_T = 26.6$. The release position (at 12:00 of July 4 and 6, respectively) of the floats located inside/outside the PPAG areas is marked with a circle/triangle. Starting position and trajectory are coloured according to depth.

relatively flat and the flow is southward. In their ascent the floats rotate anticlockwise and progress inshore until they reach the coastal jet where isopycnal outcrops, rapidly rotate clockwise and continue southward within the ML (Fig. 11a). Two days later, the floats that upwell in the same zone have similar trajectories, except that their starting depth is shallower (15–20 m) and initial flow direction is shoreward (Fig. 11c). Another difference is in the trajectories of the floats that upwell in the periphery of the filament, whose direction is clearly inshore on July 9 contrasting with the southward flow two days before.

4. Summary and discussion

Satellite data and results from a regional ocean numerical model were used to describe the spatial and temporal evolution of sea surface temperature, [Chl] concentration and advection patterns during one upwelling event off central Portugal, a region characterised by complex coastal morphology and bathymetry. The advective and stratification conditions throughout the event were characterised using the hydrodynamical model results and the three-dimensional Lagrangian displacements over 3-day periods.

The comparison between the spatio-temporal SST variability computed from the satellite data and the model, showed the model ability to realistically reproduce the main upwelling circulation features such as the filament formation off Capes Carvoeiro and Roca associated to the separation of the coastal jet, and the persistence of a warm water pool in Setúbal Bay. The main differences between the model and satellite SST patterns were the SST values in the filaments and their extension, with lower SSTs and greater filaments in the model than satellite images. It was also observed a faster and stronger SST warming in the satellite data than the model during the relaxation phase indicating that restratification of upwelled water in that model occurs on a longer timescale than observed on satellite images. Similar results were also obtained by Kuebel Cervantes and Allen (2006) in their modeling study of the upwelling off California, who reported that model temperatures tend to be cooler than in situ (mooring) temperatures, with maximum differences during periods of wind relaxation. These authors relate it with the weaker velocity relaxation response which, in turn, they attribute to their use of spatially uniform winds. The importance of spatial variability of the wind field was also stressed by Capet et al. (2004) who argued that the two most important wind properties that should be adequately determined are the strength of nearshore curl and speed drop-off near the coast. The low SSTs along the filament axis suggest that the 15 km resolution of the regional atmospheric model used here is still too coarse to adequately resolve the wind speed drop-off near the coast leading to excessive coastal divergence.

It was shown that the spatial relationship between SST, [Chl] and the advective patterns is not fixed during course of the upwelling event. When the intensity of the northerly wind component was higher than 5 m/s, there is an asymmetry between the [Chl] and surface temperature distributions, with low [Chl] values along the cold filament axis and higher [Chl] values along the southern filament boundaries. This asymmetric [Chl] distribution is a common reported feature (e.g. Jones et al., 1988; Castro et al., 2000; Moita et al., 2003) and is usually

interpreted as a result of low horizontal advection conditions. Our results suggest that mixed layer thickness plays a major role in setting the physical conditions for phytoplankton accumulation/growth and reveal other aspects of this asymmetry: the possibility for phytoplankton growth/accumulation along the northern filament boundary, as observed in the Carvoeiro filament, the general upwelling conditions also found in the areas of high [Chl] as revealed by the upward displacements in the model results, and its temporal variability with the rapid evolution to a symmetric [Chl] distribution relative to SST as soon as the northerly wind ceases.

The close relation between the high [Chl] areas and the advection conditions shows that the study of event-scale phytoplankton dynamics, in an upwelling system with complex coastal morphology and bathymetry, critically depends on the ability to realistically model the hydrodynamics at the sub-mesoscale.

The results obtained here are consistent with previous results on phytoplankton communities which showed that the upper layers of coastal waters are often characterised by the co-occurrence of pelagic phytoplankton species with high growth rates (e.g. *Chaetoceros, Thalassiosira*) and species from the benthic domain (e.g. *Paralia sulcata, Navicula, Diploneis*), forming an assemblage with high phytoplankton biomass (Estrada and Blasco, 1985; Moita, 2001). The model reproduced well this feature showing that PPAG areas are the target of floats from various depths. On the other hand, the different circulation patterns presented for Lisbon and Setúbal bays partially explain what has been reported concerning the HABs dynamics in the two bays: some HAB species can concentrate along the inshore side of the Roca filament and reach threshold concentrations for bloom initiation inside Lisbon bay (Moita et al., 2003), a feature that was not yet observed in Setúbal bay. Here, the developing of a *Lingulodinium polyedrum* bloom in 1996, inside the stratified warmer water pool, was associated with particular conditions, when the upwelling plumes rooted at capes Roca/Espichel were unusually displaced shoreward into Setúbal Bay, due to the influence of the offshore mesoscale circulation (Amorim et al., 2004). In mid July 2005, a red tide of *L. polyedrum* was reported in cape Sines, progressed northward into Setúbal bay and was later on detected in the southern side of Lisbon bay in early August. This poleward transport between Setúbal and Lisbon bays is in agreement with the pattern reproduced by the model from July 7 to 9 (Figs. 7a and b).

The results obtained here suggest that the following issues should be further investigated:

- What is the relative importance of submesoscale dynamics and coastal divergence in nutrient pumping to the euphotic zone and the maintenance of high phytoplankton concentrations observed in the shadow areas?
- What is the spatio-temporal variability of the density domes in the lee of the capes and its relationship with the duration, intensity and spatial structure of the wind forcing?
- What is the role of the above structures on the fate of the upwelled water parcels: do they remain long near surface or are they subducted quickly?

The categorisation of importance of submesoscale processes in the enrichment of the surface layers using realistic model configurations, satellite data and observations of the mesoscale processes within the water column, should improve our understanding to which extent the volume transport upwelling index may represent the variability in shelf productivity of coastal upwelling systems.

Acknowledgements

This work was supported by the FCT Project (ProFit-PDCTE/CTA/50386/ 2003). The satellite-derived sea surface temperature maps (SEVIRI and AVHRR) were obtained from the EUMETSAT's Ocean and Sea Ice Satellite Application Facility, generated at CMS (Météo-France Satellite Meteorology Centre, Lannion, Brittany, France) and distributed by IFREMER. NCEP reanalysis data provided by the NOAA/OAR/ESRL PSD, Boulder, Colorado, USA, from their Web site at http://www.cdc.noaa.gov. MODIS data were obtained from NASA/Goddard Space Flight Centre from the Web site at http://oceancolor.gsfc.nasa.gov. The ETOPO5 digital data base of land and sea-floor elevations was obtained from NGDC, Data Announcement 88-MGG-02, Digital relief of the Surface of the Earth. NOAA, National Geophysical Data Centre, Boulder, Colorado, 1988. The authors wish to acknowledge use of the Ferret program for analysis and graphics in this paper. Ferret is a product of NOAA's Pacific Marine Environmental Laboratory (information is available at www.ferret.noaa.gov). Thanks are due to Tiago Marques for his helpful review of the manuscript.

References

Amorim, A., Moita, T., Oliveira, P., 2004. Dinoflagellate blooms related to coastal upwelling plumes off Portugal. In: Steidinger, K., Landsberg, J., Thomas, C., Vargo, G. (Eds.), Harmful Algae 2002. Florida Fish and Wildlife Conservation Commission, Florida Institute of Oceanography, Intergovernmental Oceanographic Commission of UNESCO, pp. 89–91.

Capet, X., Marchesiello, P., McWilliams, J., 2004. Upwelling response to coastal wind profiles. Geophysical Research Letters 13, L13311.

Castro, C., Pérez, F., Álvarez-Salgado, X., Fraga, F., 2000. Coupling between the thermohaline, chemical and biological fields during two contrasting upwelling events off the NW Iberian Peninsula. Continental Shelf Research 20, 189–210.

CMS, 2005. North atlantic regional sea surface temperature product manual. Mto-France Satellite Meteorology Center, Lannion, Brittany, France. SAF/OSI/M-F/TEC/MA/124. ⟨http://www.osi-saf.org/biblio/docs/ss1_pmnarsst_1_7.pdf⟩.

Estrada, M., Blasco, D., 1985. Phytoplankton assemblages in coastal upwelling areas. In: Bas, C., Margalef, R., Rubias, P. (Eds.), International Symposium of Upwelling of W. Africa, vol. 1. Instituto de Investigationes Pesqueras, Barcelona, pp. 379–402.

Feldman, G.C., McClain, C.R., 2006. Ocean color web, modis reprocessing 1.1. NASA Goddard Space Flight Center. In: Kuring, N., Bailey, S.W. (Eds.), vol.11, December 2006. ⟨http://oceancolor.gsfc.nasa.gov⟩.

Fiúza, A., 1983. Upwelling patterns off Portugal. In: Suess, E., Thiede, J. (Eds.), Coastal Upwelling: Its Sediment Record, Part A. Plenum Press, New York, pp. 85–98.

Haidvogel, D., Beckmann, A., 1999. Numerical Ocean Circulacion Modeling. Imperial College Press.

Haynes, R., Barton, E., Pilling, I., 1993. Development, persistence, and variability of upwelling filaments off the Atlantic coast of the Iberian Peninsula. Journal of Geophysical Research 98 (C12), 22681–22692.

Jones, B., Atkinson, L., Blasco, D., Brink, K., Smith, S., 1988. The asymmetric distribution of chlorophyll associated with a coastal upwelling center. Continental Shelf Research 8 (10), 1155–1170.

Kalnay, E., et al., 1996. The NCEP/NCAR 40-Year Reanalysis Project. Bulletin of the American Meteorological Society 77.

Kuebel Cervantes, B., Allen, J., 2006. Numerical model simulations of continental shelf flows off northern California. Deep Sea Research Part II 53, 2956–2984.

Largier, J., Lawrence, C., Roughan, M., Kaplan, D., Dever, E., Dorman, C., Kudela, R., Bollens, S., Wilkerson, F., Dugdale, R., Botsford, L., Garfield, N., Kuebel Cervantes, B., Koracin, D., 2006. WEST: A northern California study of the role of wind-driven transport in the productivity of coastal plankton comunities. Deep Sea Research Part II 53, 2833–2849.

Levy, M., 2008. The modulation of biological production by oceanic mesoscale turbulence, vol. 744. Lecture Notes in Physics. Springer, Berlin, pp. 219–261, doi:10.1007/978-3-540-75215-8_9.

Marchesiello, P., Estrade, P., 2007. Eddy activity and mixing in upwelling systems: a comparative study of Northwest Africa and California regions. International Journal of Earth Sciences 1, 1.

Marta-Almeida, M., Dubert, J., 2006. The structure of tides in the western Iberian region. Continental Shelf Research 26, 385–400.

Moita, M., 2001. Estrutura, variabilidade e dinâmica do fitoplâncton na costa de Portugal continental. Ph.D. Thesis, Universidade de Lisboa, pp. 272.

Moita, T., Oliveira, P., Mendes, J., Palma, A., 2003. Distribution of chlorophyll *a* and *gymnodinium catenatum* associated with coastal upwelling plumes off central Portugal. Acta Oecologica 24, S125–S132.

Morel, A., Berthon, J., 1989. Surface pigments, algal biomass profiles, and potential production of the euphotic layer: relationships reinvestigated in view of remote-sensing applications. Limnology and Oceanography 34, 1545–1562.

Peliz, A., Fiúza, A., 1999. Temporal and spatial variability of CZCS-derived phytoplankton pigment concentrations off western Iberian Peninsula. International Journal of Remote Sensing 20 (7), 1363–1403.

Peliz, A., Dubert, J., Marchesiello, P., Teles-Machado, A., 2007a. Surface circulation in the Gulf of Cadiz: model and mean flow structure. Journal of Geophysical Research 112, C11015.

Peliz, A., Marchesiello, P., Dubert, J., Marta-Almeida, M., Roy, C., Queiroga, H., 2007b. A study of crab larvae dispersal on the Western Iberian Shelf: physical processes. Journal of Marine Systems 68, 215–236.

Penven, P., Debreu, L., Marchesiello, P., McWilliams, J., 2006. Evaluation and application of the ROMS 1-way embedding procedure to the central California upwelling system. Ocean Modelling 12, 157–187.

Shchepetkin, A., McWilliams, J., 2003. A method for computing horizontal pressure-gradient force in an oceanic model with a nonaligned vertical coordinate. Journal of Geophysical Research 108 (C3), 3090.

Shchepetkin, A.F., McWilliams, J.C., 2005. The regional oceanic modeling system (ROMS): a split-explicit, free-surface, topography-following-coordinate oceanic model. Ocean Modelling 9 (4), 347–404.

Skamarock, W.C., Klemp, J.B., Dudhia, J., Gill, D.O., Barker, D.M., Wang, W., Powers, J.G., 2005. A description of the Advanced Research WRF Version 2. Technical Report, MMMD-NCAR, Boulder, Colorado, USA.

Smith, W., Sandwell, D., 1997. Global sea floor topography from satellite altimetry and ship depth soundings. Science 277 (5334), 1956–1962.

Sousa, F., Bricaud, A., 1992. Satellite-derived phytoplankton structures in the Portuguese upwelling area. Journal Geophysical Research 97 (C7), 11343–11356.

Teles-Machado, A., Peliz, A., Dubert, J., Sanchez, R., 2007. On the onset of the Gulf of Cadiz Coastal Contercurrent. Geophysical Research Letters 34, L12601.

Wilkin, J.L., Arango, H., Haidvogel, D.B., Lichtenwalner, C.S., Glenn, S.M., Headström, K.S., 2005. A regional ocean modeling system for the long-term ecosystem observatory. Journal of Geophysical Research 110.